2023-05-20

Ocean circulation and biological processes drive seasonal variations of dissolved Al, Cd, Ni, Cu, and Zn on the Northeast Atlantic continental margin

Chen, X-G

10.1016/j.marchem.2023.104246
Marine Chemistry
Elsevier BV

[Geophysical Research Letters]

Supporting Information for

Ocean circulation and biological processes drive seasonal variations of dissolved Al, Cd, Ni, Cu, and Zn on the Northeast Atlantic continental margin

Xue-Gang Chen[1,2*#], Dagmara Rusiecka[1,3#], Martha Gledhill[1,3], Angela Milne[4], Amber L. Annett[3], Antony J. Birchill[4,5], Maeve C. Lohan[3], Simon Ussher[4], E. Malcolm S. Woodward[6], Eric P. Achterberg[1,3*]

[1] GEOMAR Helmholtz Centre for Ocean Research Kiel, Kiel, Germany,

[2] Ocean College, Zhejiang University, Zhoushan, China

[3] Ocean and Earth Sciences, National Oceanography Centre, University of Southampton, Southampton, UK

[4] School of Geography, Earth and Environmental Sciences, University of Plymouth, Plymouth, UK

[5] School of Environment, Geography and Geosciences, University of Portsmouth, UK.

[6] Plymouth Marine Laboratory, Plymouth, UK

Corresponding authors:

Xue-Gang Chen, xchen@geomar.de, chenxg83@zju.edu.cn

Eric P. Achterberg, eachterberg@geomar.de

Both authors contribute equal to this paper.

Contents of this file

Methods

Dissolved trace metals:

Seawater samples were collected using 24 × 10 L Teflon coated Trace metal clean Ocean Test Equipment (OTE) bottles positioned on a Titanium frame rosette system. All OTE bottles were pressurized with filtered (0.2 µm PTFE, Millex-FG 50, Millipore) compressed air. Seawater samples were filtered in-line using a 0.2 µm membrane filter capsule (Sartorius, Sartobran P) into acid washed 125 ml Low-density polyethylene bottles. All samples were acidified to pH of ~ 1.8 with ultra-pure hydrochloric acid (UpA Romil) in the laminar flow hood bench and stored double-bagged in ziplock bags.

Seawater samples for dissolved trace metal (dTM) analyses were described in Rapp et al. (2017). In detail, seawater samples were sub-sampled (15 ml) into fluorinated ethylene propylene bottles in the laminar flow hood bench. All sample bottles were spiked with 100 µL of diluted spike. Then, seawater samples were pre-concentrated by automated system (SC-4 DX SeaFast pico; ESI) with online pH buffering and seawater sample matrix removal. Preconcentrated samples were analyzed by high-resolution inductively coupled plasma-mass spectrometry (HR-ICP-MS; Thermo Fisher Element XR) in low resolution (R = 300) for ^{110}Cd, ^{111}Cd, ^{115}In and in medium resolution (R = 4000) for ^{60}Ni, ^{62}Ni, ^{63}Cu, ^{65}Cu, ^{66}Zn, and ^{68}Zn. Reference materials, SAFe GEOTRACES S and D1 were used to check the accuracy and precision of the measurements and the results are consistent with consensus values (Table S1).

Dissolved Al (dAl):

Seawater samples for dAl were sub-sampled (5 mL) into acid washed 50 ml plastic tubes. An aluminum spectrofluorometric complex was obtained with addition of lumogallion (Hydes & Liss, 1976) at pH of 5.0 - 5.5 adjusted by addition of ammonium acetate buffer as per Rapp et al. (2017) and heated for 3 hours at 55°C. Samples were analyzed by a spectrofluorometer (The Cary Eclipse Fluorometer). The measured dAl concentrations of a reference standard (GS) were consistent with consensus values (Table S1).

Radium isotopic activities ($^{223}Ra_{xs}$, $^{224}Ra_{xs}$):

Large volume samples for radium (Ra) analysis were collected from Niskin bottles deployed on a stainless-steel frame. Seawater samples for Ra were transferred into acid-washed 20 L collapsible containers, and passed slowly (<750 mL min^{-1}) through a column filled with 20 g of MnO_2-impregnated acrylic fiber

to extract Ra from seawater (Moore, 2008). Fibers were rinsed with ultra-high purity water to remove salts, and partially dried to optimize emanation of the radon daughter (Sun & Torgersen, 1998). Then, seawater samples were counted immediately using a Radium Delayed Coincidence Counter [RaDeCC; (Moore, 2008; Moore & Arnold, 1996). Counting was repeated after an interval of ~30 (~90) days to determine the ^{224}Ra (^{223}Ra) activity supported by the parent isotopes ^{228}Th (^{227}Ac). Uncertainty calculations followed the methods of Garcia-Solsona et al. (2008). The efficiencies of the RaDeCC systems were calibrated and monitored using standards prepared from ^{227}Ac and ^{232}Th (Annett et al., 2013). Radium activities used here ($^{224}Ra_{xs}$ and $^{223}Ra_{xs}$) are in excess of activity supported by the parent isotopes in water columns.

Nutrients:

Unfiltered seawater samples for nutrients (nitrate+nitrite (TN), phosphate (P), silicic acid (Si)) were taken from the same OTE bottles as trace metal samples. They were stored in 'aged' 10% HCl acid washed and Milli-Q rinsed high-density polyethylene bottles. Seawater sampling and handling for nutrient analysis was carried out according to the International GO-SHIP nutrient manual recommendations (Hydes et al., 2010). Nutrient analysis was carried out on board within few hours of sampling using techniques described in Woodward & Rees (2001).

Physical Oceanography:

Conductivity, temperature, and depth (CTD) data were collected and processed on board. Turbidity was measured by an Aquatrack MKIII fluorometer (Chelsea Technologies Group) at a wavelength 400 nm and a bandwidth of 80 nm. Salinity was measured by a Sea-Bird SBE 4C sensor and calibrated on-board using in-situ salinity samples analyzed with a Guildline Autosal salinometer. Temperature was measured with Sea-Bird SBE 3plus (SBE 3P) temperature sensor. Dissolved oxygen was measured by a Sea-Bird SBE 43 oxygen sensor and calibrated against photometric on-board Winkler titration results. Apparent oxygen utilization (AOU) is calculated from the presumed oxygen concentrations under atmospheric saturation for a given temperature (θ) and salinity (S), subtracted from the observed dissolved oxygen concentrations.

$$AOU = \left[O_{2,sat}(\theta, S)\right] - [O_2]$$

Statistics and plots

Figs. 1, 2, 3, and Fig. S12 were created with the Ocean Data View (5.6.2) software (Schlitzer, 2021)

using DIVA gridding.

All other plots and associated statistics were performed by *R* programming 4.2.0 with packages *tidyverse* (Wickham et al., 2019), psych (Revelle, 2017), and *ggpmisc* (Aphalo, 2022).

Hydrography

The mixing of water masses were quantified using extended Optimum Multiparameter analysis (extOMP) (Hupe & Karstensen, 2000; Karstensen & Tomczak, 1998; Pollard et al., 2004). The full details of the extOMP analysis and related results have been reported by Rusiecka et al. (2018). Five different water masses (Fig. S1, Fig. S8) were identified in the study region from top to bottom: a seasonal mixed layer (SML) and East North Atlantic Central Waters (ENACW), Sub-Arctic Intermediate Waters (SAIW), Mediterranean Outflow Waters (MOW), Labrador Sea Water (LSW) and North East Atlantic Deep Waters (NEADW). These observations were consistent with previous reports from the study region (Cotté-Krief et al., 2002).

The SML is defined as the depth with temperature changes $|\Delta T| = 0.2$ °C relative to the shallowest temperature. The depth of SML varied between 40 – 103 m in November, 30 – 170 m in April and 20 – 30 m in July, suggesting the highest water column stratification in July. The lowest sea surface temperature was measured in April because of the winter water column overturning and heat loss to the atmosphere during winter.

Below the SML with depths down to ~ 500 m (< 27.30 kg m^{-3} σ_0), the water columns are mainly consisted of ENACW, followed by SAIW and MOW. At intermediate depths ~ 500 – 1500 m (27.30 – 27.78 m^{-3} σ_0,), a distinctive salinity maximum, significant contribution of MOW was observed (García-Ibáñez et al., 2015; McCartney, 1992). The MOW are formed at the Strait of Gibraltar where Mediterranean Sea deep waters mix with ENACW and sink to a depth of ~ 1000 m to form a neutrally buoyant plume that spreads across the North East Atlantic (García-Ibáñez et al., 2015). In our study region, salinity (~ 35.62) and temperature (~ 9.1 ºC) at the maximum MOW contribution (~ 27.62 kg m^{-3} σ_0, depth ~ 1000 m) were consistently lower across all seasons in comparison to salinity (35.61 – 36.36) and temperature (7.57 – 12.18 ºC) of MOW in the Gulf of Cadiz (GEOTRACES GA04 section) (Rolison, 2016). This indicates mixing of bottom layers of MOW with colder (3.30ºC) and less saline (34.87) LSW and/or SAIW that share similar

density range with MOW (Johnson & Gruber, 2007; Talley & McCartney, 1982). At density > 27.78 kg m^{-3}, the water columns are mainly consisted of LSW, SAIW, and NEADW. The LSW is formed in the Labrador and Irminger sea (van Aken, 2000b; Paillet et al., 1998; Pickart et al., 2003), while the SAIW is produced by the mixing between the warm and saline North Atlantic Current with the cold and fresher LSW in the subpolar gyre (van Aken, 2000a; Arhan, 1990). The bottom waters on Celtic Sea was gradually increasingly contributed by colder NEADW (1.98 ºC) that generated from the mixing of various subpolar mode waters and Iceland – Scotland Overflow Water (van Aken, 2000a; García-Ibáñez et al., 2018). Accordingly, the contribution of SAIW and MOW gradually decreases with increasing depth of bottom waters.

The absolute contributions of water masses change with their defined endmember characteristics. Here, we focus on the connection between kinks of metal:P ratios and water mass contributions. Hence, our discussions are largely based on the vertical profiles of water masses and the junctions of water mass contributions (e.g., at density of 27.62 kg m^{-3}), rather than the absolute contributions of each water mass. Changing the weights and stoichiometries of defined water masses does not produce significant variations in the overall vertical profiles of water masses on the NE Atlantic continental margin. Furthermore, the high correlations between dTMs and water mass contributions and the extremely low residuals (measured – modeled) dTMs indicate that our water mass analysis is robust to reconstruct the dTM distributions at depth.

Supporting Figures

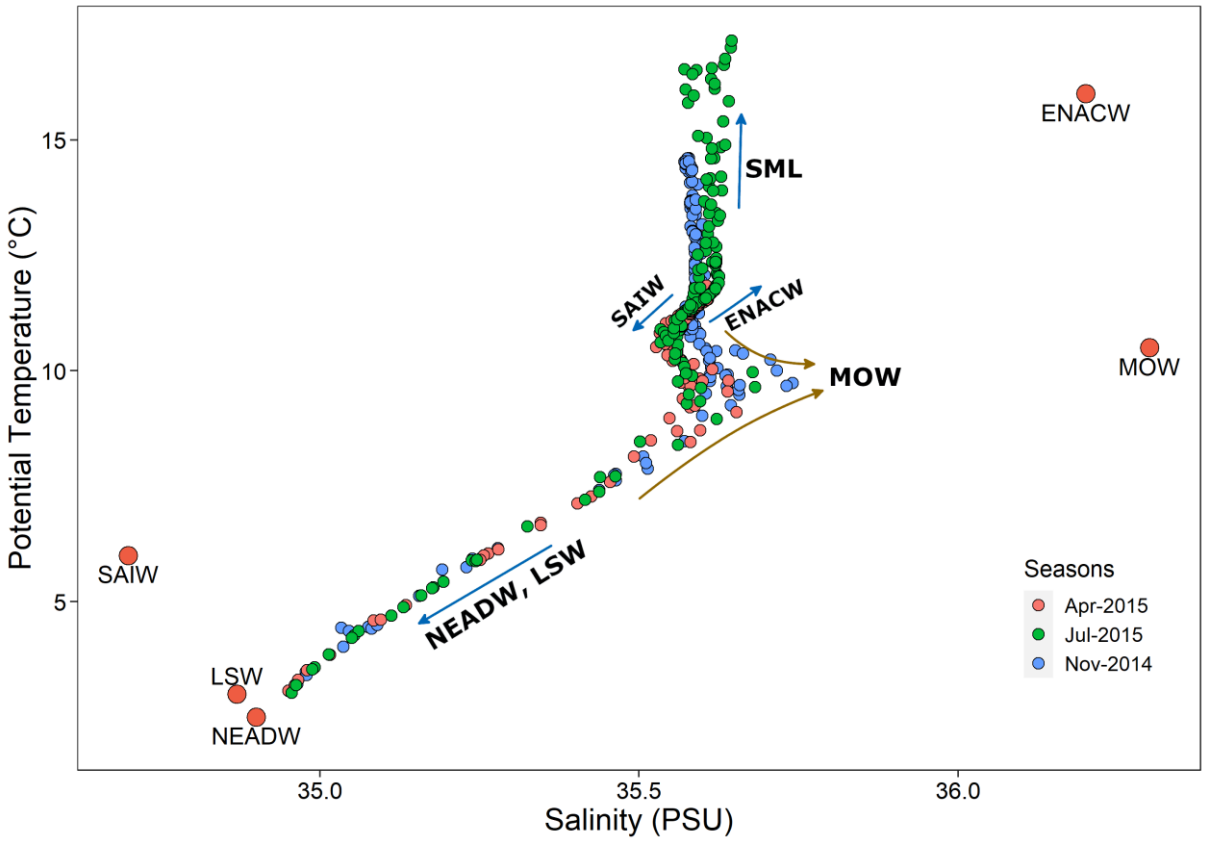

Fig. S1: Θ-S plot of water columns on the continental slope of Celtic Sea. The assigned potential temperature and salinity of water masses are acquired from García-Ibáñez et al. (2015) and GLODAP v2 (Olsen et al., 2019) as per Rusiecka et al. (2018). ENACW: East North Atlantic Central Waters, SAIW: Sub-Arctic Intermediate Waters, MOW: Mediterranean Outflow Waters, LSW: Labrador Sea Water, NEADW: North East Atlantic Deep Waters.

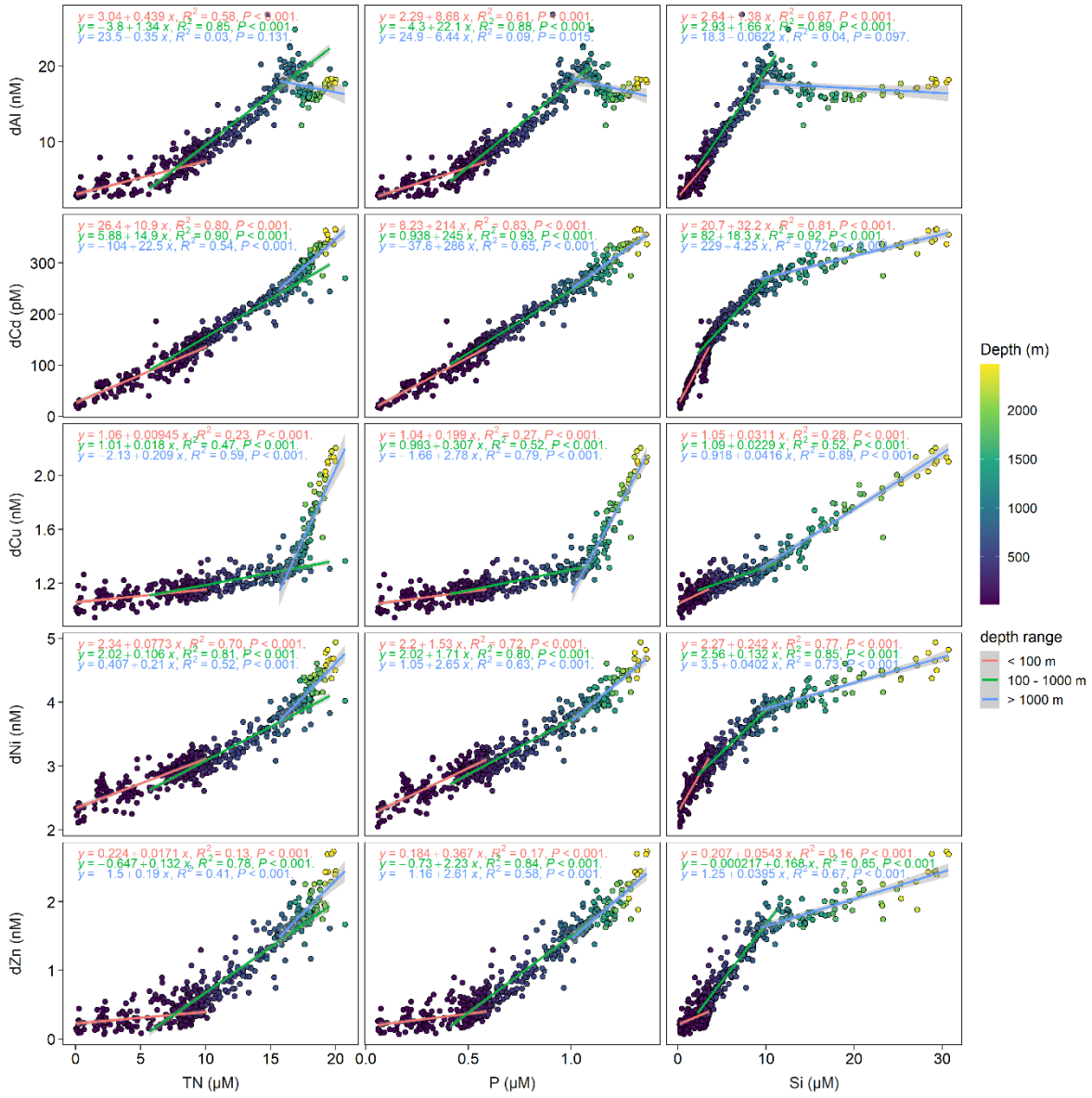

Fig. S2: Correlations between dissolved trace metals (dAl, dCd, dCu, dNi, dZn) and nutrients (nitrate+nitrite (TN), phosphate (P), silicic acid (Si)) on the continental slope of Celtic Sea. Linear regression models are applied to surface (< 100 m), 100 – 1000 m (density generally 27.25 – 27.62 kg m^{-3}), and > 1000 m (density > 27.62 kg m^{-3}), respectively.

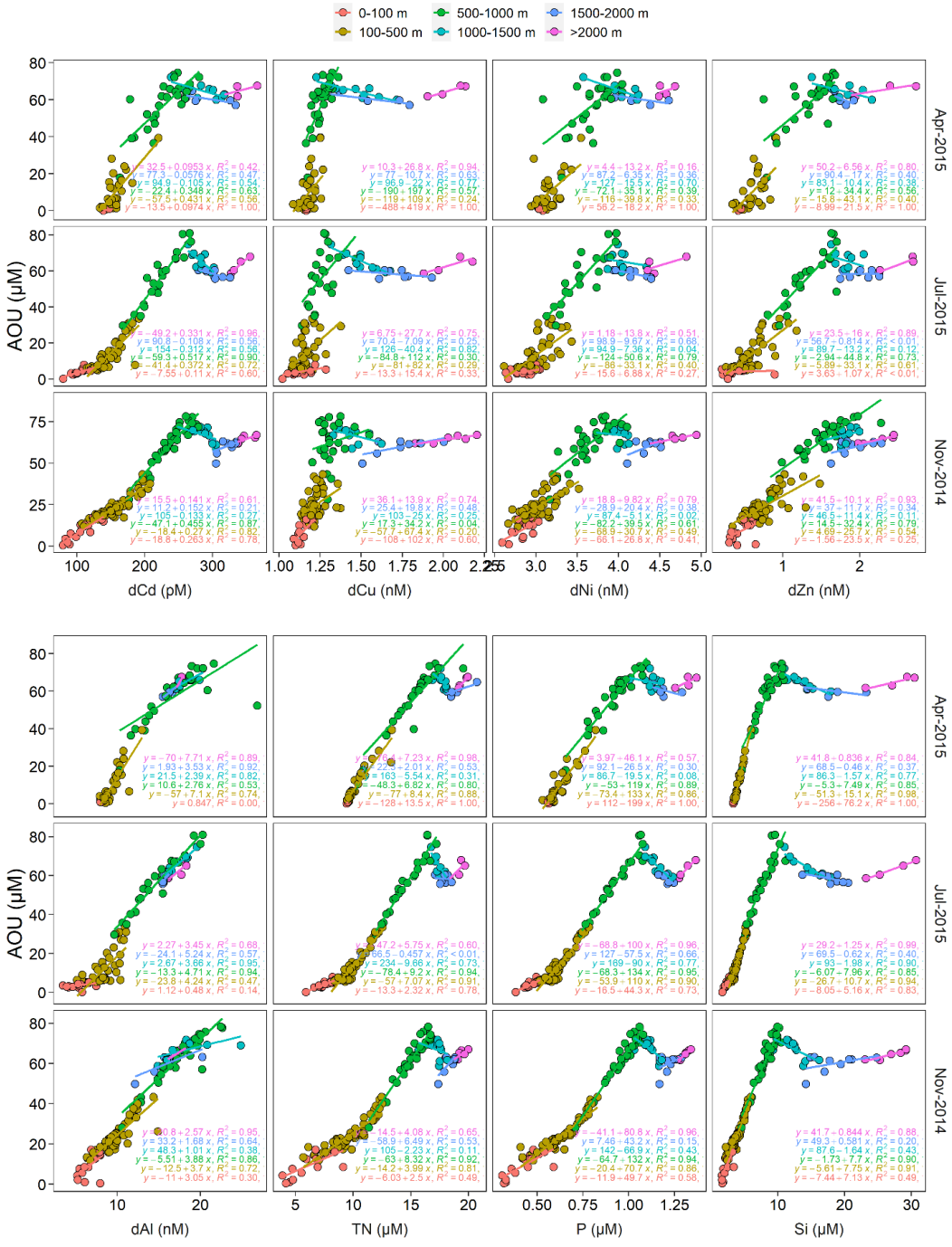

Fig. S3: Correlations between dissolved trace metals (dAl, dCd, dCu, dNi, dZn) and nutrients (nitrate+nitrite (TN), phosphate (P), silicic acid (Si)) and apparent oxygen utilization (AOU) on the continental slope of Celtic Sea. Linear regression models are applied to each defined depth range as distinguished by their colors.

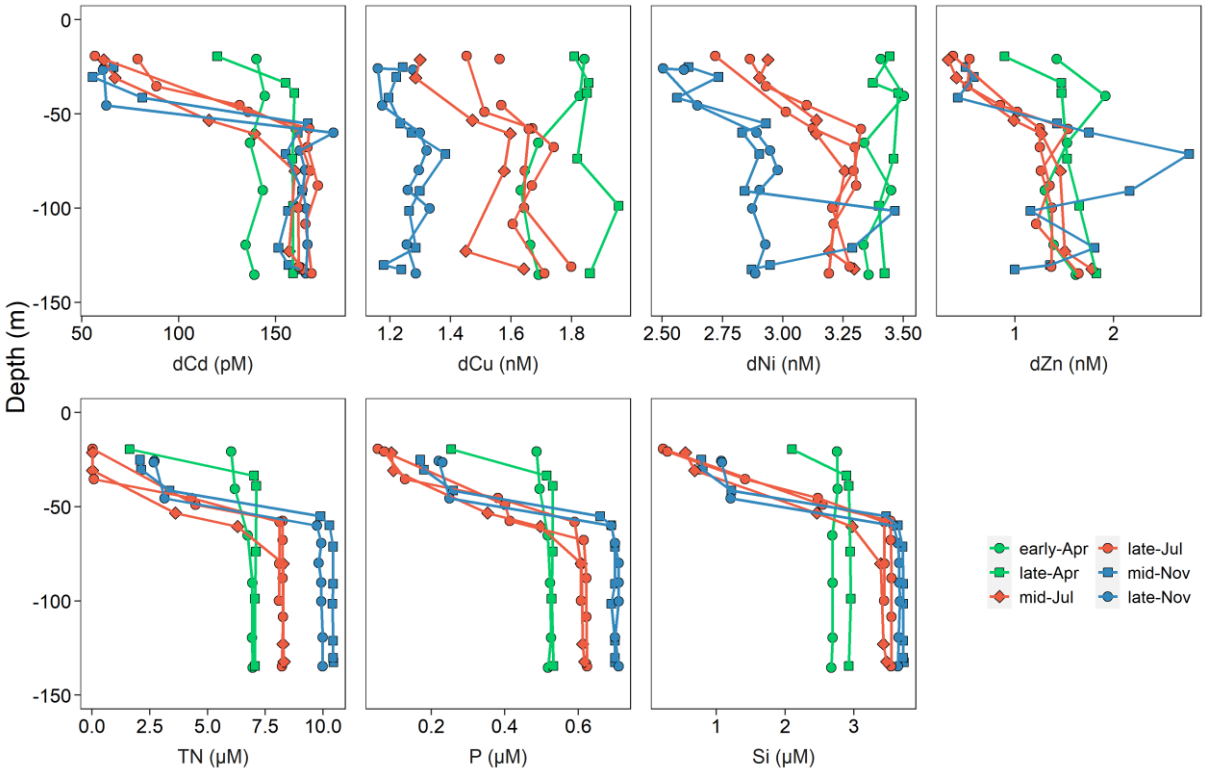

Fig. S4: Seasonal variations of dissolved trace metal (dTMs: dCd, dCu, dNi, dZn) and nutrient (nitrate+nitrite (TN), phosphate (P), silicic acid (Si)) concentrations of water columns at station CCS (central Celtic Sea). Note that some *x* ranges are not starting from 0.

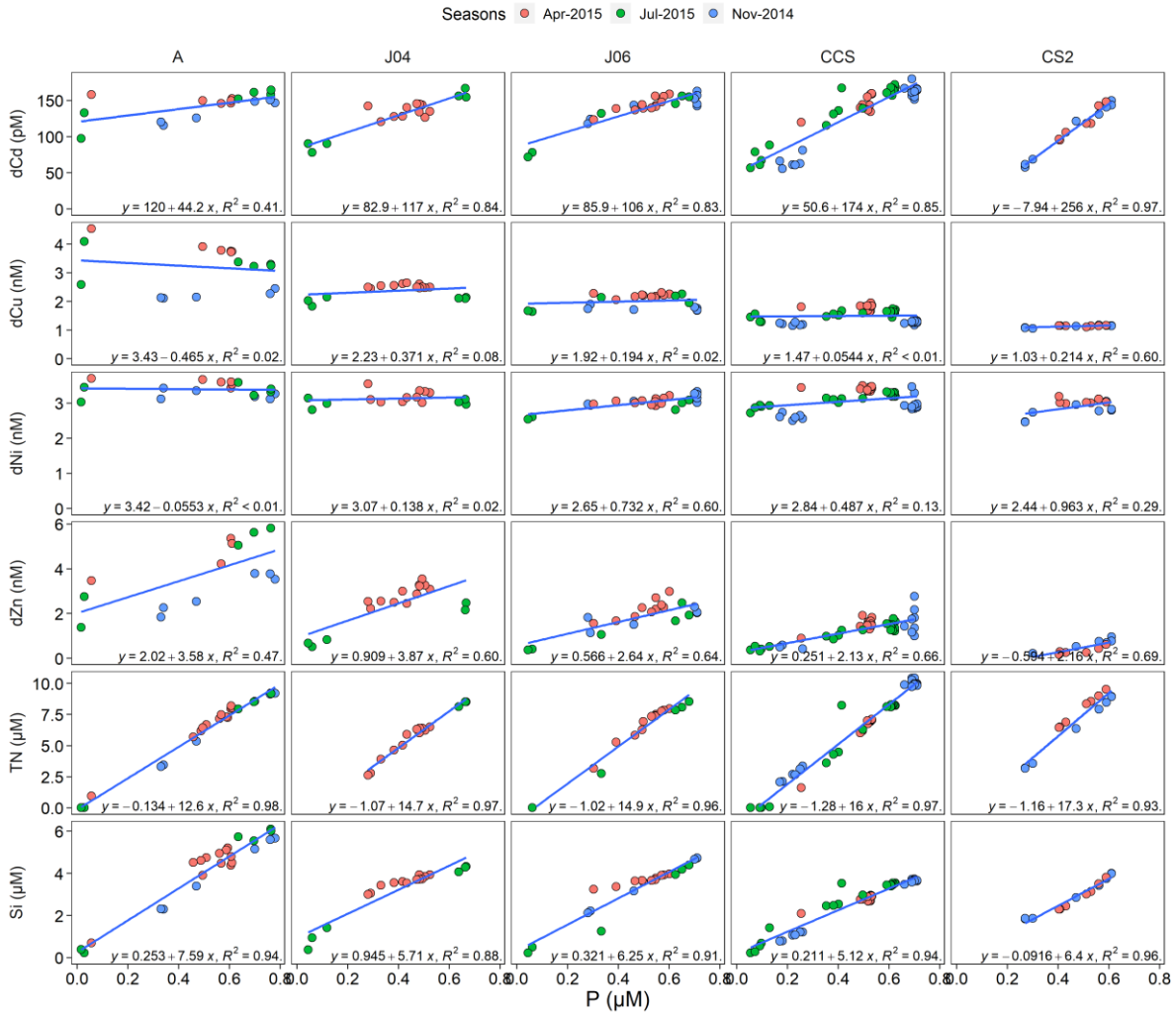

Fig. S5: Variations of dissolved trace metal (dCd, dCu, dNi, dZn) – phosphate (P), nitrate+nitrite (TN) – P, and silicic acid (Si) – P correlations with stations on the continental shelf of Celtic Sea.

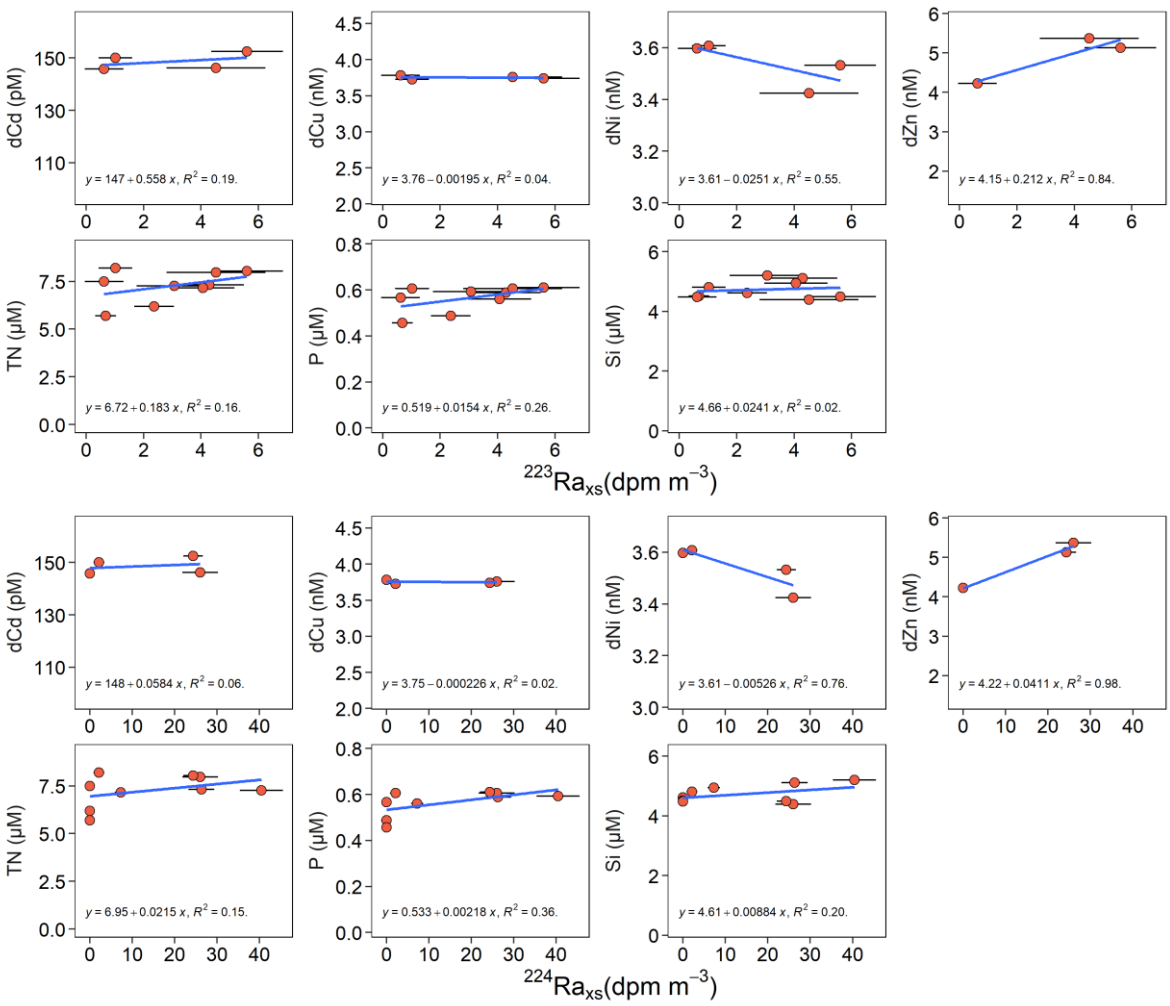

Fig. S6: Correlations between dissolved trace metal (dCd, dCu, dNi, dZn) and nutrient (nitrate+nitrite (TN), phosphate (P), silicic acid (Si)) concentrations and radium isotopic activities ($^{223}Ra_{xs}$ and $^{224}Ra_{xs}$) on the continental shelf of Celtic Sea.

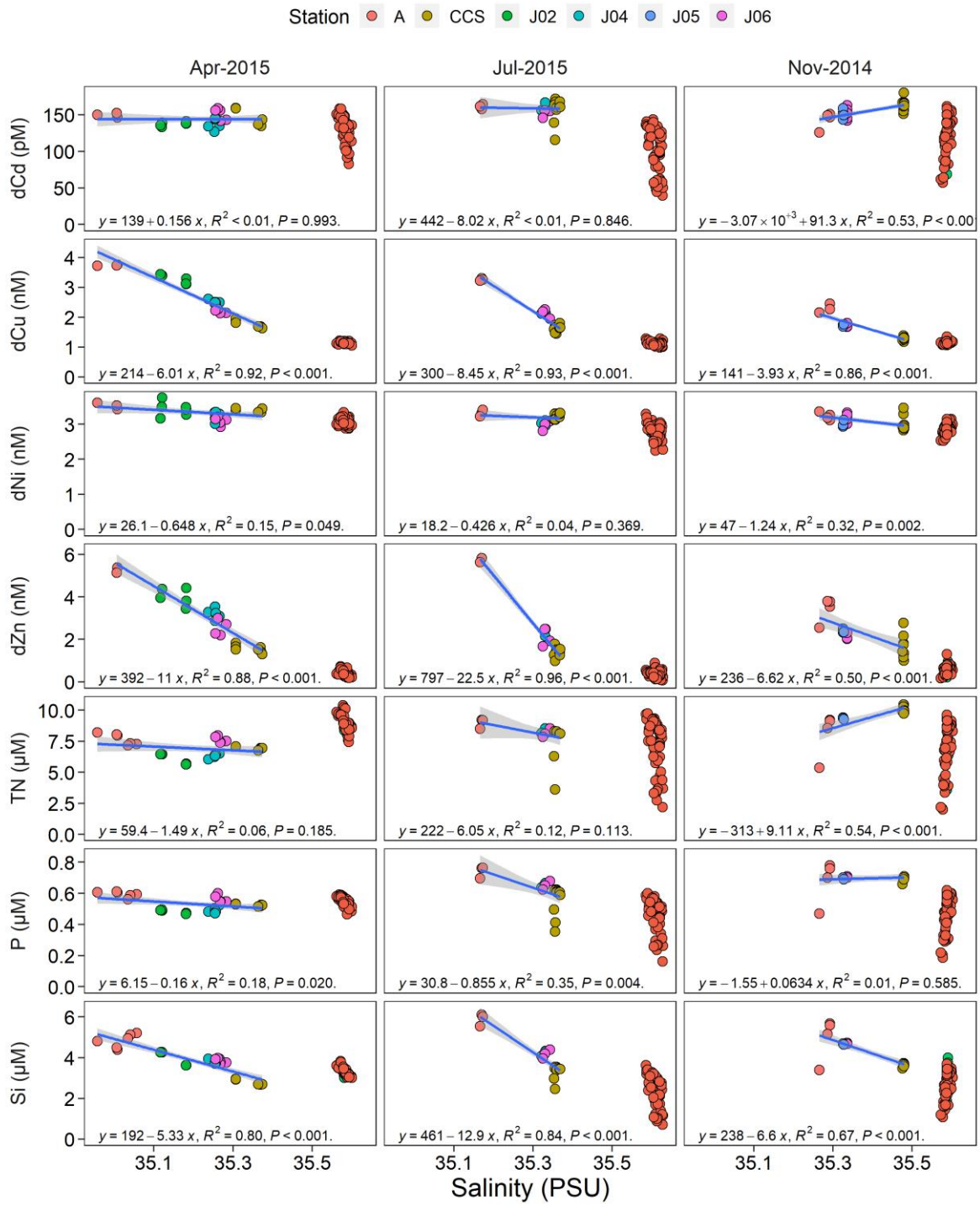

Fig. S7: Correlations between subsurface (depth of 50 – 200 m) dissolved trace metal (dCd, dCu, dNi, dZn) and nutrient (nitrate+nitrite (TN), phosphate (P), silicic acid (Si)) concentrations with salinity on the continental shelf and slope of the Northeast Atlantic Ocean.

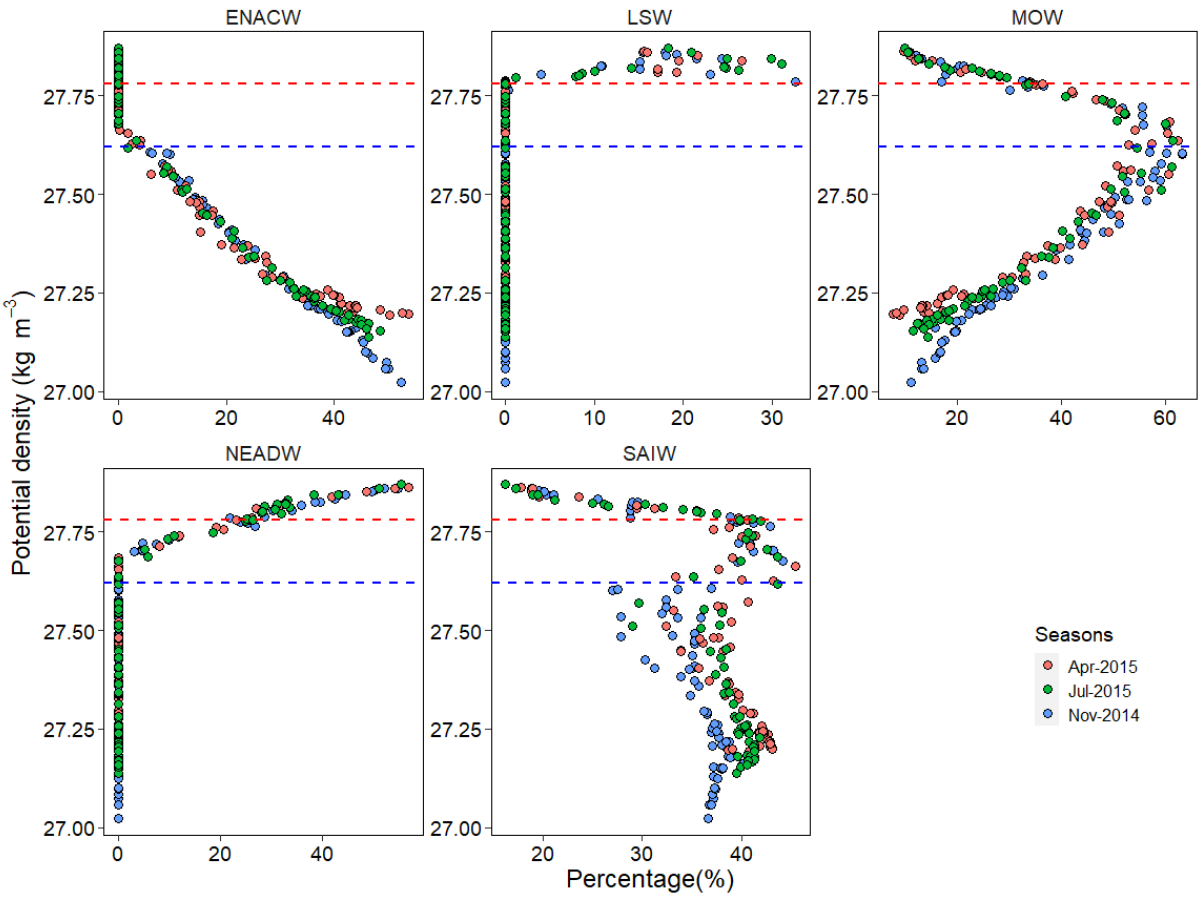

Fig. S8: Percentage contributions of water masses for the water columns on the continental slope of Celtic Sea. Water mass contributions were calculated using extOMP analyses as per Rusiecka et al. (2018) (See the supporting methods for more details). Surface waters (depths < 200 m) were excluded from extOMP calculation. The red and blue dashed lines indicate important junctions between water masses at potential density of ~ 27.78 kg m^{-3} (depth ~ 1500 m) and ~ 27.62 kg m^{-3} (depth ~ 1000 m), respectively. ENACW: East North Atlantic Central Waters, SAIW: Sub-Arctic Intermediate Waters, MOW: Mediterranean Outflow Waters, LSW: Labrador Sea Water, NEADW: North East Atlantic Deep Waters.

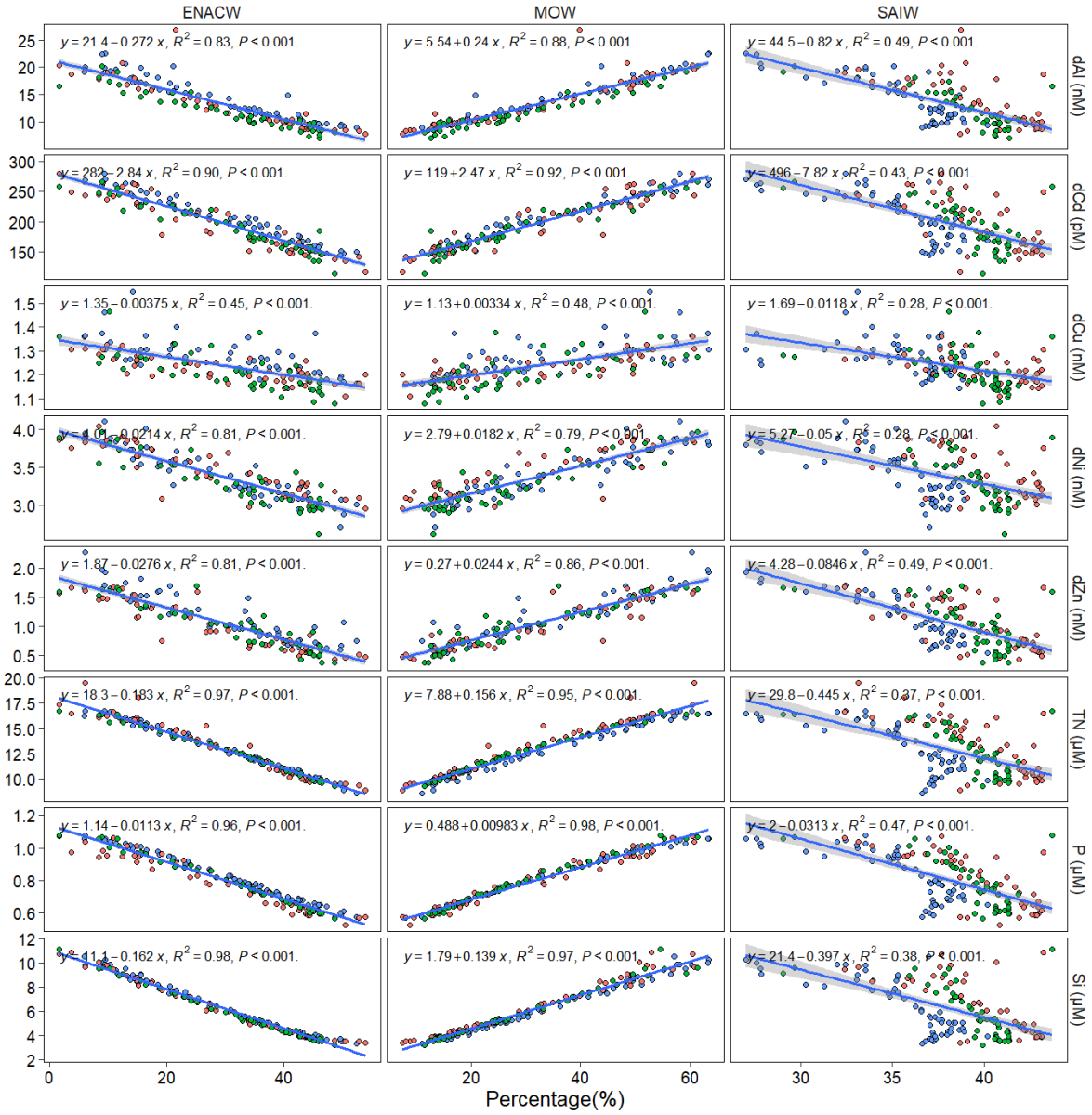

Fig. S9: Correlations between dissolved trace metal (dAl, dCd, dCu, dNi, dZn) and nutrient (nitrate+nitrite (TN), phosphate (P), silicic acid (Si)) concentrations and water mass contributions on the continental slope of Celtic Sea. Water columns with potential density < 27.62 kg m^{-3} (depths of < ~ 1000 m) were chosen to estimate the endmember concentrations of Mediterranean Outflow Waters (MOW).

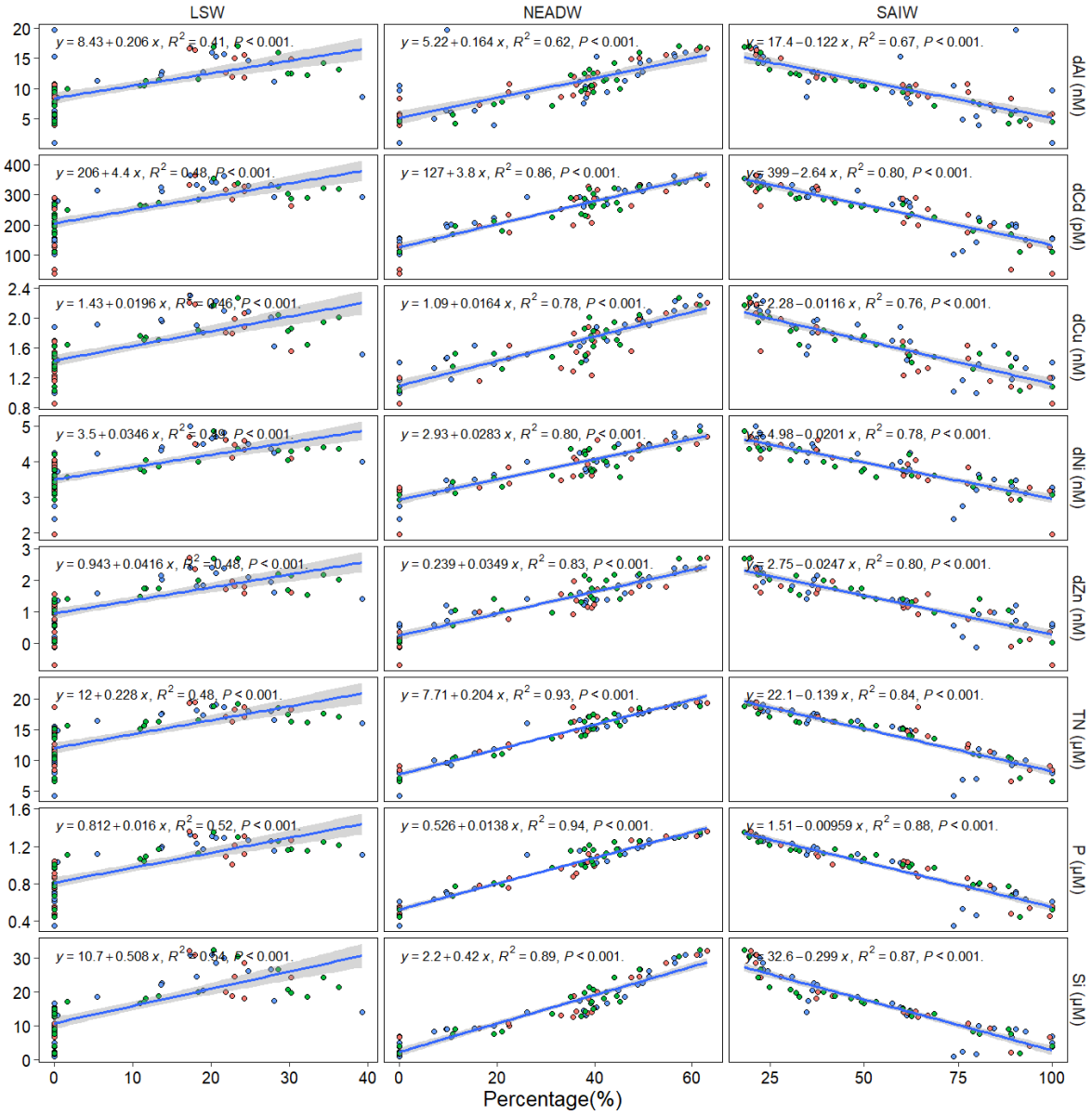

Fig. S10: Correlations between dissolved trace metal (dTM: dAl, dCd, dCu, dNi, dZn) and nutrient (nitrate+nitrite (TN), phosphate (P), silicic acid (Si)) concentrations and water mass contributions on the continental slope of Celtic Sea. The dTM and nutrient concentrations and water mass contributions have been corrected by removing the Mediterranean Outflow Waters (MOW) contributions (MOW endmember calculated from Fig. S9). Water columns with potential density > 27.62 kg m^{-3} (depths > ~ 1000 m) were chosen to calculate the endmember concentrations of Sub-Arctic Intermediate Waters (SAIW).

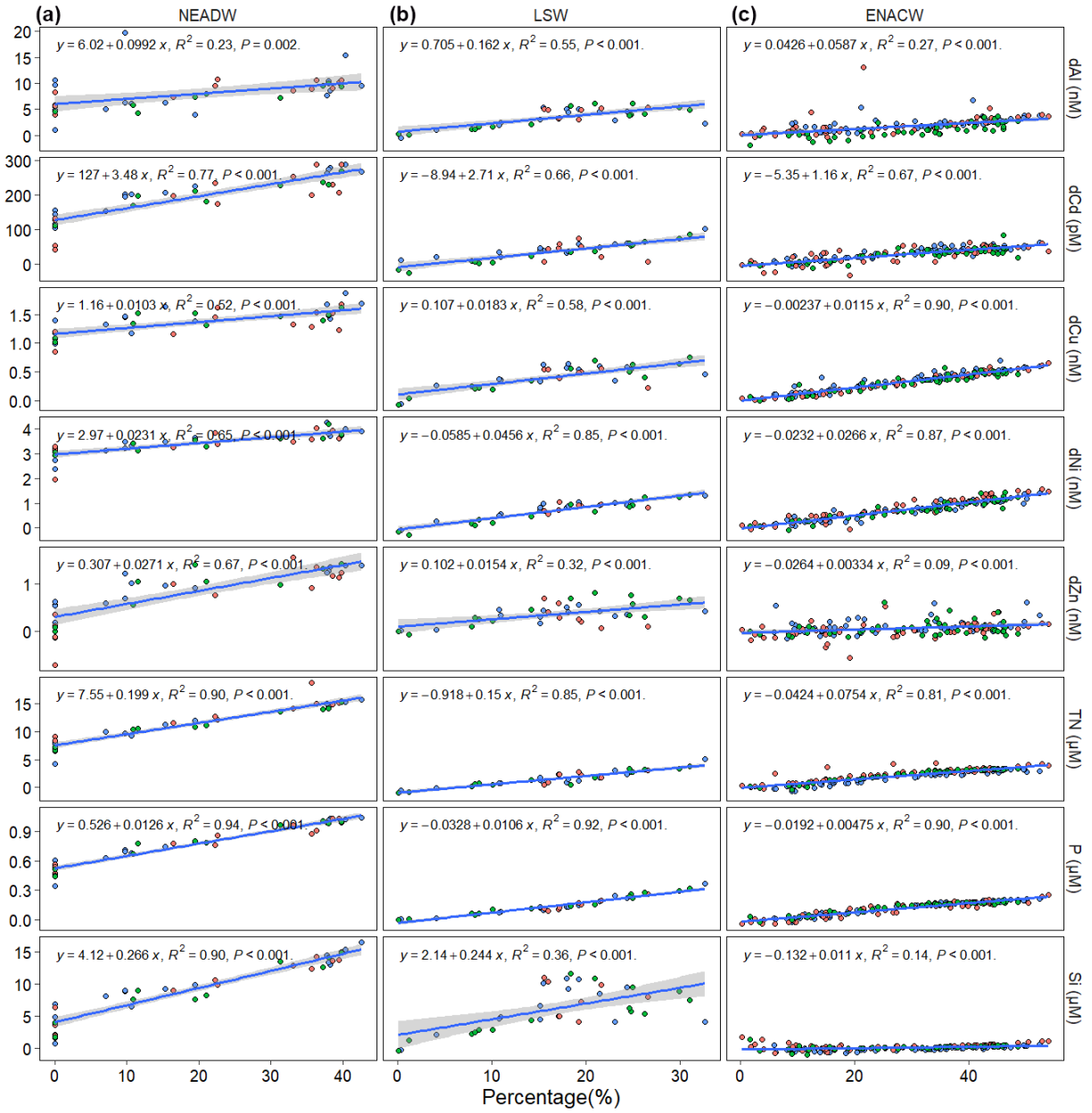

Fig. S11: Correlations between dissolved trace metal (dTM: dAl, dCd, dCu, dNi, dZn) and nutrient (nitrate+nitrite (TN), phosphate (P), silicic acid (Si)) concentrations and water mass contributions on the continental slope of Celtic Sea. (a) The dTM and nutrient concentrations and water mass contributions have been corrected by removing the Mediterranean Outflow Waters (MOW) contributions (MOW endmember calculated from Fig. S9). Water columns with depths of > ~ 1000 m and Labrador Sea Water (LSW) contribution < 1% were chosen to calculate the North East Atlantic Deep Waters (NEADW) endmember. (b) and (c): The dTM and nutrient levels contributed from MOW, Sub-Arctic Intermediate Waters (SAIW),

and NEADW were subtracted based on their endmember concentrations. The dTMs and nutrients were only provided by LSW at depth > ~ 1000 m (b) and by East North Atlantic Central Waters (ENACW) at depths < ~ 1000 m (c).

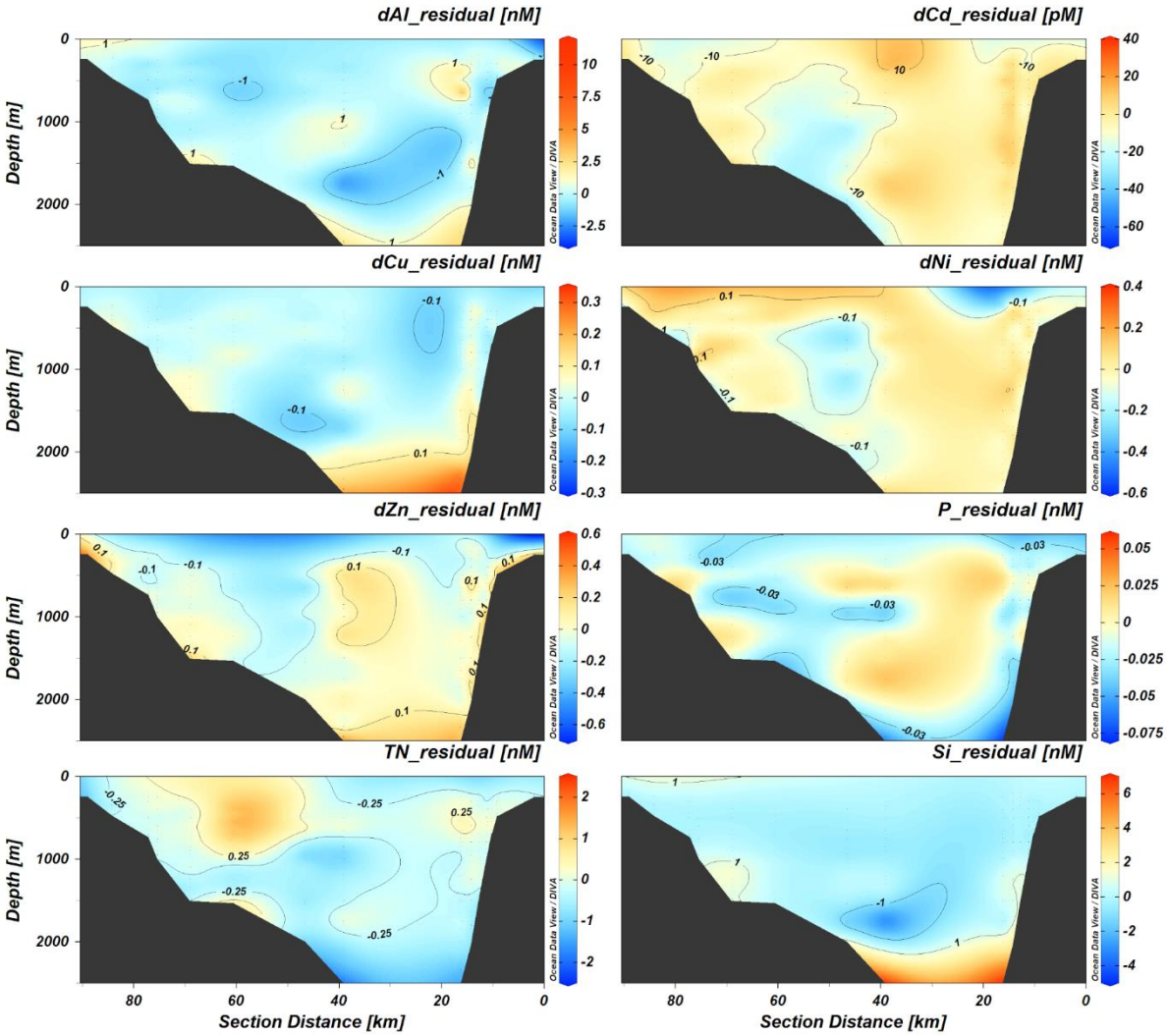

Fig. S12: The residuals (measured – modeled) of dTMs and nutrients along the slope transect.

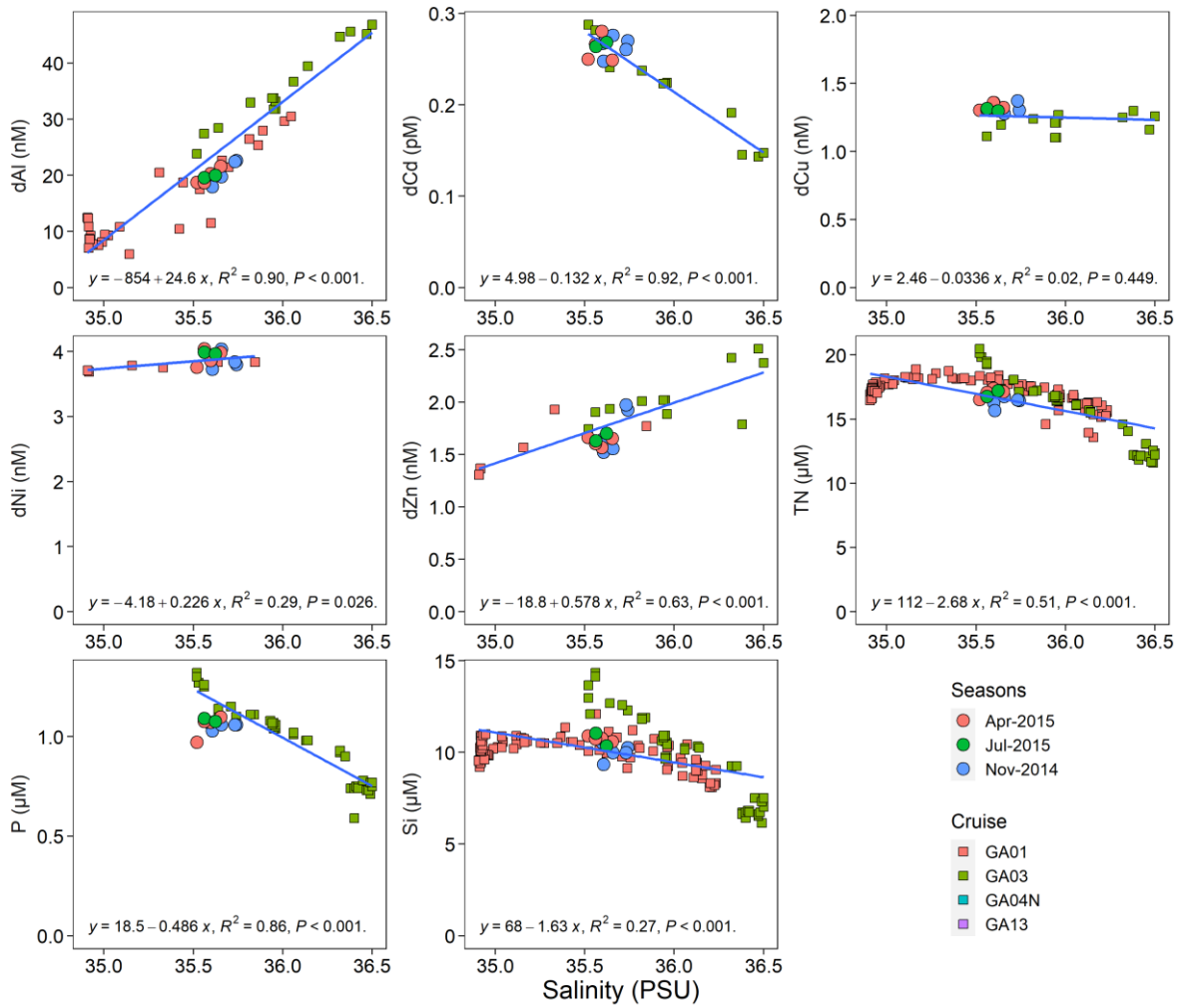

Fig. S13: Variations of dissolved trace metals (dAl, dCd, dCu, dNi, dZn) and nutrients (nitrate+nitrite (TN), phosphate (P), silicic acid (Si)) with salinity on the Northeast Atlantic Ocean. In order to cover the core of MOW, the depths were assigned to 900 – 1400 m for published data of the Northeast Atlantic Ocean (GEOTRACES Intermediate Data Product Group, 2021) and 950 – 1050 m for this study.

Supporting Tables

Table S1 GEOTRACES reference material results for dissolved Cd (dCd), Ni (dNi), Cu (dCu), Zn (dZn), and Al (dAl).

	dCd (pM)	**dNi (nM)**	**dCu (nM)**	**dZn (nM)**	**dAl (nM)**
Reported SAFe S		2.32 ± 0.22 (n=10)	0.705 ± 0.130 (n=8)	0.071 ± 0.025 (n=8)	
Reported SAFe D1	979 ± 145 (n=17)	8.41 ± 0.14 (n=15)	2.19 ± 0.06 (n=15)	7.13 ± 0.22 (n=19)	
Consensus SAFe S		2.28 ± 0.09	0.52 ± 0.05	0.069 ± 0.010	
Consensus SAFe D1	991 ± 31	8.58 ± 0.26	2.27 ± 0.11	7.40 ± 0.35	
Reported GS					27.0 ± 0.6 (n = 6)
Consensus GS					27.5 ± 0.2

Consensus values obtained from https://www.geotraces.org/standards-and-reference-materials/.

Table S2: Seasonal variations of dissolved trace metal and nutrient concentrations (min – max (mean ± sd)) on the Northeast Atlantic continental slope at different depth ranges.

Nutrient	Seasons	Depth ranges					
		< 30 m	**50 - 100 m**	**100 - 500 m**	**500 - 1000 m**	**1000 - 1500 m**	**> 1500 m**
dAl (nM)	Apr-2015	3.05 - 7.9 (5.97±1.55)	5.48 - 8.6 (7.28±0.87)	7.21 – 13.0 (8.96±1.17)	10.3 - 26.8 (17.0±3.1)	16.3 - 20.3 (18.1±1.4)	15.5 - 17.9 (17.0±0.8)
	Jul-2015	2.76 - 5.39 (3.29±0.70)	2.81 - 7.47 (4.58±1.30)	5.18 - 11.1 (8.62±1.40)	9.66 - 20.3 (14.8±3.0)	15.7 - 19.6 (17.1±1.3)	15.5 - 18.3 (16.4±1.1)
	Nov-2014	4.13 - 5.69 (4.83±0.48)	3.9 - 7.95 (6.18±1.22)	6.34 - 14.9 (9.89±1.76)	10.6 - 22.6 (17.6±2.8)	14.9 - 24.9 (18.4±2.6)	12.1 - 20.3 (16.4±1.8)
dCd (pM)	Apr-2015	40 - 186 (107±35)	82.7 - 150.7 (121±18)	112 - 220 (148±18)	164 - 281 (230±30)	239 - 317 (286±26)	262 - 366 (314±36)
	Jul-2015	15.6 - 51.2 (27.5±10.1)	39.6 - 126 (85.7±25.8)	115 - 192 (148±20)	168 - 268 (224±27)	264 - 302 (283±12)	279 - 356 (314±23)
	Nov-2014	57.7 - 80.6 (66.4±7.1)	57.4 - 139 (96.2±24.6)	107 - 208 (156±25)	177 - 280 (241±24)	248 - 305 (286±16)	300 - 365 (331±19)
dCu (nM)	Apr-2015	1.06 - 1.19 (1.12±0.04)	1.05 - 1.20 (1.14±0.03)	1.09 - 1.27 (1.17±0.04)	1.16 - 1.36 (1.26±0.05)	1.23 - 1.72 (1.46±0.15)	1.32 - 2.14 (1.77±0.30)
	Jul-2015	0.979 - 1.26 (1.04±0.07)	0.985 - 1.29 (1.10±0.07)	1.08 - 1.38 (1.16±0.06)	1.14 - 1.47 (1.26±0.07)	1.32 - 1.68 (1.51±0.11)	1.42 - 2.18 (1.81±0.22)
	Nov-2014	1.05 - 1.14 (1.10±0.03)	1.01 - 1.21 (1.14±0.05)	1.14 - 1.38 (1.21±0.05)	1.20 - 1.55 (1.32±0.07)	1.33 - 1.63 (1.45±0.08)	1.51 - 2.20 (1.86±0.21)
dNi (nM)	Apr-2015	2.87 - 3.19 (3.02±0.10)	2.87 - 3.22 (3.04±0.09)	2.94 - 3.55 (3.14±0.13)	3.08 - 4.04 (3.69±0.24)	3.57 - 4.24 (4.03±0.20)	3.95 - 4.68 (4.38±0.27)
	Jul-2015	2.05 - 2.87 (2.35±0.21)	2.25 - 3.05 (2.7±0.223)	2.61 - 3.43 (3.02±0.17)	3.13 - 3.97 (3.56±0.26)	3.87 - 4.34 (4.02±0.13)	3.94 - 4.82 (4.29±0.24)
	Nov-2014	2.46 - 2.76 (2.61±0.10)	2.53 - 3.03 (2.80±0.14)	2.66 - 3.52 (3.0±0.18)	3.17 - 4.10 (3.67±0.23)	3.73 - 4.13 (4.01±0.11)	4.10 - 4.94 (4.47±0.22)
dZn (nM)	Apr-2015	0.156 - 0.574 (0.32±0.16)	0.188 - 0.660 (0.35±0.11)	0.302 - 0.911 (0.54±0.14)	0.748 - 1.68 (1.33±0.29)	1.38 - 2.16 (1.78±0.23)	1.67 - 2.73 (1.98±0.36)
	Jul-2015	0.089 - 0.443 (0.22±0.09)	0.070 - 0.895 (0.32±0.17)	0.262 - 1.18 (0.59±0.20)	0.801 - 1.70 (1.32±0.28)	1.63 - 2.05 (1.82±0.13)	1.75 - 2.70 (2.15±0.31)
	Nov-2014	0.183 - 0.442 (0.30±0.09)	0.177 - 0.647 (0.42±0.14)	0.343 - 1.48 (0.75±0.21)	0.837 - 2.28 (1.48±0.32)	1.52 – 2.00 (1.80±0.12)	1.63 - 2.44 (2.08±0.27)

Nitrate+Nitrite (µM)	Apr-2015	5.62 - 8.58 (7.41±1.01)	7.42 - 10.1 (8.77±0.57)	8.57 - 13.4 (9.94±1.03)	10.9 - 19.6 (15.5±1.7)	16.9 - 18.1 (17.8±0.4)	18.0 - 20.7 (19.2±0.8)
	Jul-2015	0.054 - 2.66 (0.701±0.818)	2.19- 8.41 (6.12±1.86)	8.12 - 12.6 (9.99±1.18)	12.0 - 17.2 (14.7±1.5)	16.8 - 18.1 (17.4±0.4)	17.1 - 19.7 (18.3±0.8)
	Nov-2014	1.66 - 4.03 (2.91±0.98)	2.00 - 9.16 (5.26±1.98)	5.69 - 12.5 (9.53±1.68)	11.4 - 16.8 (15.1±1.3)	15.7 - 18.2 (17.2±0.6)	17.4 – 20.0 (18.7±0.7)
Phosphate (µM)	Apr-2015	0.326 - 0.507 (0.45±0.06)	0.466 - 0.581 (0.53±0.03)	0.513 - 0.819 (0.60±0.06)	0.655 - 1.10 (0.93±0.11)	1.00 - 1.19 (1.13±0.05)	1.13 - 1.37 (1.25±0.08)
	Jul-2015	0.059 - 0.208 (0.10±0.05)	0.162 - 0.516 (0.39±0.10)	0.498 - 0.783 (0.62±0.08)	0.745 - 1.08 (0.93±0.11)	1.09 - 1.24 (1.15±0.05)	1.16 - 1.37 (1.24±0.06)
	Nov-2014	0.180 - 0.300 (0.24±0.05)	0.186 - 0.590 (0.38±0.108)	0.410 - 0.830 (0.63±0.10)	0.710 - 1.08 (0.97±0.09)	1.03 - 1.18 (1.12±0.04)	1.17 - 1.34 (1.25±0.06)
Silicic acid (µM)	Apr-2015	2.30 - 3.36 (2.87±0.27)	3.01 - 3.54 (3.22±0.14)	3.14 - 6.04 (3.82±0.58)	4.70 - 10.9 (8.41±1.62)	11.0 – 18.0 (13.7±2.0)	13.8 - 30.5 (22.0±6.2)
	Jul-2015	0.230 - 0.839 (0.43±0.20)	0.708 - 2.77 (1.88±0.63)	2.70 - 5.38 (3.77±0.80)	5.13 - 11.2 (7.85±1.69)	11.0 - 17.9 (14.0±2.4)	13.7 - 30.7 (21.0±5.1)
	Nov-2014	1.05 - 1.86 (1.38±0.27)	1.08 - 3.44 (2.11±0.65)	2.24 - 5.98 (3.82±0.91)	4.60 - 10.5 (8.36±1.43)	9.35 - 16.2 (12.6±1.7)	14.3 - 29.2 (21.8±5.3)

Table S3 Variations of metal:P ratios with depth along the continental slope of Celtic Sea

Depth range	**dAl:P (mmol mol^{-1})**	**dCd:P (µmol mol^{-1})**	**dCu:P (mmol mol^{-1})**	**dNi:P (mmol mol^{-1})**	**dZn:P (mmol mol^{-1})**
< 100 m	8.68 ± 0.55	214 ± 8	0.199 ± 0.026	1.53 ± 0.08	0.367 ± 0.065
100 – 1000 m	22.1 ± 0.6	245 ± 4	0.307 ± 0.020	1.71 ± 0.06	2.23 ± 0.07
> 1000 m	Highly variable	286 ± 26	2.78 ± 0.18	2.65 ± 0.25	2.61 ± 0.28

Table S4 Estimated endmember concentrations (with 95% confidence levels) of water masses on the Northeast (NE) Atlantic Ocean. ENACW: East North Atlantic Central Waters, SAIW: Sub-Arctic Intermediate Waters, MOW: Mediterranean Outflow Waters, LSW: Labrador Sea Water, NEADW: North East Atlantic Deep Waters.

Water mass	**dAl (nM)**	**dCd (pM)**	**dCu (nM)**	**dNi (nM)**	**dZn (nM)**	**P* (µM)**	**P (µM)**	**TN* (µM)**	**TN (µM)**	**Si* (µM)**	**Si (µM)**
ENACW	5.91 ± 1.13	111 ± 9	1.15 ± 0.05	2.64 ± 0.12	0.31 ± 0.13	0.10	0.46 ± 0.02	0.1	7.50 ± 0.42	0.85	0.97 ± 0.31
SAIW	5.17 ± 1.04	134 ± 16	1.12 ± 0.08	2.96 ± 0.13	0.28 ± 0.15	0.86	0.55 ± 0.04	13.0	8.22 ± 0.74	6.3	2.68 ± 1.38
MOW	29.6 ± 1.0	366 ± 9	1.47 ± 0.04	4.61 ± 0.11	2.71 ± 0.12	1.20	1.47 ± 0.02	17.5	23.5 ± 0.4	9.0	15.7 ± 0.3
MOW[1]	35.6 ± 6.8	202 ± 45	1.21 ± 0.07	-	1.99 ± 0.24		0.96 ± 0.18		15.5 ± 2.5		9.6 ± 2.3
MOW[2]		~ 160		~ 4	~ 2						
MOW[3]	20.1 ± 1.5	264 ± 11	1.32 ± 0.03	3.90 ± 0.11	1.68 ± 0.14		1.06 ± 0.03		16.7 ± 0.5		10.4 ± 0.5
LSW	16.9 ± 4.2	262 ± 56	1.94 ± 0.44	4.50 ± 0.55	1.65 ± 0.65	1.05	1.03 ± 0.09	16.5	14.1 ± 1.7	10.0	26.6 ± 9.4
NEADW	15.9 ± 4.9	475 ± 53	2.20 ± 0.27	5.28 ± 0.46	3.02 ± 0.54	1.65	1.79 ± 0.09	22.5	27.4 ± 1.8	45.0	30.7 ± 2.5
NEADW[4]	23.1 ± 2.3	372 ± 14	2.75 ± 0.12	5.40 ± 0.05	3.02 ± 0.29		1.49 ± 0.03		22.3 ± 0.4		45.0 ± 1.5

* Pre-determined nutrient concentrations, adopted from García-Ibáñez et al. (2015) and GLODAP v2 (Olsen et al., 2019) following Rusiecka et al. (2018).

[1] Calculated from the water columns with depths of 900 – 1400 m near the Gibraltar channel where the occurrence of MOW is significant (Middag et al., 2022; Rolison et al., 2015). Data obtained from (GEOTRACES Intermediate Data Product Group, 2021).

[2] From Middag et al. (2022).

[3] Average values of water columns with depths of 950 – 1050 m on the NE Atlantic continental slope (this study).

[4] Calculated from water columns with depths of > 4000 m on the NE Atlantic Ocean. Data obtained from (GEOTRACES Intermediate Data Product Group, 2021).

References

van Aken, H. M. (2000a). The hydrography of the mid-latitude northeast Atlantic Ocean: I: The deep water masses. *Deep Sea Research Part I: Oceanographic Research Papers*, *47*(5), 757–788. https://doi.org/10.1016/S0967-0637(99)00092-8

van Aken, H. M. (2000b). The hydrography of the mid-latitude Northeast Atlantic Ocean: II: The intermediate water masses. *Deep Sea Research Part I: Oceanographic Research Papers*, *47*(5), 789–824. https://doi.org/10.1016/S0967-0637(99)00112-0

Annett, A. L., Henley, S. F., Van Beek, P., Souhaut, M., Ganeshram, R., Venables, H. J., et al. (2013). Use of radium isotopes to estimate mixing rates and trace sediment inputs to surface waters in northern Marguerite Bay, Antarctic Peninsula. *Antarctic Science*, *25*(03), 445–456. https://doi.org/10.1017/S0954102012000892

Aphalo, P. J. (2022). ggpmisc: Miscellaneous Extensions to "ggplot2." Retrieved from https://docs.r4photobiology.info/ggpmisc/

Arhan, M. (1990). The North Atlantic Current and Subarctic Intermediate Water. *Journal of Marine Research*, *48*(1), 109–144. https://doi.org/10.1357/002224090784984605

Charette, M. A., Morris, P. J., Henderson, P. B., & Moore, W. S. (2015). Radium isotope distributions during the US GEOTRACES North Atlantic cruises. *Marine Chemistry*, *177*, 184–195. https://doi.org/10.1016/j.marchem.2015.01.001

Cotté-Krief, M.-H., Thomas, A. J., & Martin, J.-M. (2002). Trace metal (Cd, Cu, Ni and Pb) cycling in the upper water column near the shelf edge of the European continental margin (Celtic Sea). *Marine Chemistry*, *79*(1), 1–26. https://doi.org/10.1016/S0304-4203(02)00013-0

Elderfield, H., & Rickaby, R. E. M. (2000). Oceanic Cd/P ratio and nutrient utilization in the glacial Southern Ocean. *Nature*, *405*(6784), 305–310. https://doi.org/10.1038/35012507

García-Ibáñez, M. I., Pardo, P. C., Carracedo, L. I., Mercier, H., Lherminier, P., Ríos, A. F., & Pérez, F. F. (2015). Structure, transports and transformations of the water masses in the Atlantic Subpolar Gyre. *Progress in Oceanography*, *135*, 18–36. https://doi.org/10.1016/j.pocean.2015.03.009

García-Ibáñez, M. I., Pérez, F. F., Lherminier, P., Zunino, P., Mercier, H., & Tréguer, P. (2018). Water mass distributions and transports for the 2014 GEOVIDE cruise in the North Atlantic. *Biogeosciences*, *15*(7), 2075–2090. https://doi.org/10.5194/bg-15-2075-2018

Garcia-Solsona, E., Garcia-Orellana, J., Masqué, P., & Dulaiova, H. (2008). Uncertainties associated with 223Ra and 224Ra measurements in water via a Delayed Coincidence Counter (RaDeCC). *Marine Chemistry*, *109*(3–4), 198–219. https://doi.org/10.1016/j.marchem.2007.11.006

GEOTRACES Intermediate Data Product Group. (2021). The GEOTRACES Intermediate Data Product 2021 (IDP2021). *NERC EDS British Oceanographic Data Centre NOC*. Retrieved from 10.5285/cf2d9ba9-d51d-3b7c-e053-8486abc0f5fd

Hupe, A., & Karstensen, J. (2000). Redfield stoichiometry in Arabian Sea subsurface waters. *Global Biogeochemical Cycles*, *14*(1), 357–372. https://doi.org/10.1029/1999GB900077

Hydes, D. J., & Liss, P. S. (1976). Fluorimetric method for the determination of low concentrations of dissolved aluminium in natural waters. *Analyst*, *101*(922), 922–931. https://doi.org/10.1039/an9760100922

Hydes, D. J., Aoyama, M., Aminot, A., Bakker, K., Becker, S., Coverly, S., & Daniel, A. (2010). Determination of dissolved nutrients (N, P, Si) in seawater with high precision and inter-comparability using gas-segmented

continuous flow analysers. *In The GO-SHIP Repeat Hydrography Manual : A Collection of Expert Reports and Guidelines.*, *IOCCP No 1*(OCPO Publication Series No. 134, version 1), 1–87.

Johnson, G. C., & Gruber, N. (2007). Decadal water mass variations along 20°W in the Northeastern Atlantic Ocean. *Progress in Oceanography*, *73*(3), 277–295. https://doi.org/10.1016/j.pocean.2006.03.022

Karstensen, J., & Tomczak, M. (1998). Age determination of mixed water masses using CFC and oxygen data. *Journal of Geophysical Research: Oceans*, *103*(C9), 18599–18609. https://doi.org/10.1029/98JC00889

McCartney, M. (1992). Recirculating components to the deep boundary current of the northeern North Atlantic. *Progress in Oceanography*, *29*, 283–383.

Middag, R., Rolison, J. M., George, E., Gerringa, L. J. A., Rijkenberg, M. J. A., & Stirling, C. H. (2022). Basin scale distributions of dissolved manganese, nickel, zinc and cadmium in the Mediterranean Sea. *Marine Chemistry*, *238*, 104063. https://doi.org/10.1016/j.marchem.2021.104063

Moore, W. S. (2000). Determining coastal mixing rates using radium isotopes. *Continental Shelf Research*, *20*(15), 1993–2007. https://doi.org/10.1016/S0278-4343(00)00054-6

Moore, W. S. (2008). Fifteen years experience in measuring 224Ra and 223Ra by delayed-coincidence counting. *Marine Chemistry*, *109*(3–4), 188–197.

Moore, W. S., & Arnold, R. (1996). Measurement of 223Ra and 224Ra in coastal waters using a delayed coincidence counter. *Journal of Geophysical Research: Oceans*, *101*(C1), 1321–1329. https://doi.org/10.1029/95JC03139

Olsen, A., Lange, N., Key, R. M., Tanhua, T., Álvarez, M., Becker, S., et al. (2019). GLODAPv2.2019 – an update of GLODAPv2. *Earth System Science Data*, *11*(3), 1437–1461. https://doi.org/10.5194/essd-11-1437-2019

Paillet, J., Arhan, M., & McCartney, M. S. (1998). Spreading of Labrador sea water in the eastern North Atlantic. *Journal of Geophysical Research: Oceans*, *103*(C5), 10223–10239.

Pickart, R. S., Straneo, F., & Moore, G. K. (2003). Is Labrador Sea water formed in the Irminger basin? *Deep Sea Research Part I: Oceanographic Research Papers*, *50*(1), 23–52.

Pollard, R. T., Read, J. F., Holliday, N. P., & Leach, H. (2004). Water masses and circulation pathways through the Iceland Basin during Vivaldi 1996. *Journal of Geophysical Research: Oceans*, *109*(C4), n/a-n/a. https://doi.org/10.1029/2003JC002067

Rapp, I., Schlosser, C., Rusiecka, D., Gledhill, M., & Achterberg, E. P. (2017a). Automated preconcentration of Fe, Zn, Cu, Ni, Cd, Pb, Co, and Mn in seawater with analysis using high-resolution sector field inductively-coupled plasma mass spectrometry. *Analytica Chimica Acta*, *976*, 1–13. https://doi.org/10.1016/j.aca.2017.05.008

Rapp, I., Schlosser, C., Rusiecka, D., Gledhill, M., & Achterberg, E. P. (2017b). Automated preconcentration of Fe, Zn, Cu, Ni, Cd, Pb, Co, and Mn in seawater with analysis using high-resolution sector field inductively-coupled plasma mass spectrometry. *Analytica Chimica Acta*, *976*, 1–13. https://doi.org/10.1016/j.aca.2017.05.008

Revelle, W. R. (2017). psych: Procedures for personality and psychological research.

Rolison, J. M., Middag, R., Stirling, C. H., Rijkenberg, M. J. A., & de Baar, H. J. W. (2015). Zonal distribution of dissolved aluminium in the Mediterranean Sea. *Marine Chemistry*, *177*, 87–100. https://doi.org/10.1016/j.marchem.2015.05.001

Rolison, John Michael. (2016). *The biogeochemistry of trace metals and their isotopes in the Mediterranean and Black Seas*. (Doctoral dissertation thesis). University of Otago.

Rusiecka, D., Gledhill, M., Milne, A., Achterberg, E. P., Annett, A. L., Atkinson, S., et al. (2018). Anthropogenic Signatures of Lead in the Northeast Atlantic. *Geophysical Research Letters*, *45*(6), 2734–2743. https://doi.org/10.1002/2017GL076825

Schlitzer, R. (2021). Ocean Data View, odv.awi.de.

Schulz, K., Büttner, S., Rogge, A., Janout, M., Hölemann, J., & Rippeth, T. P. (2021). Turbulent Mixing and the Formation of an Intermediate Nepheloid Layer Above the Siberian Continental Shelf Break. *Geophysical Research Letters*, *48*(9), e2021GL092988. https://doi.org/10.1029/2021GL092988

Shi, X., Wei, L., Hong, Q., Liu, L., Wang, Y., Shi, X., et al. (2019). Large benthic fluxes of dissolved iron in China coastal seas revealed by 224Ra/228Th disequilibria. *Geochimica et Cosmochimica Acta*, *260*, 49–61. https://doi.org/10.1016/j.gca.2019.06.026

Sun, Y., & Torgersen, T. (1998). The effects of water content and Mn-fiber surface conditions on measurement by emanation. *Marine Chemistry*, *62*, 299–306. https://doi.org/10.1016/S0304-4203(98)00019-X

Talley, L. D., & McCartney, M. S. (1982). Distribution and Circulation of Labrador Sea Water. *Journal of Physical Oceanography*, *12*(11), 1189–1205. https://doi.org/10.1175/1520-0485(1982)012<1189:DACOLS>2.0.CO;2

Tian, Z., Jia, Y., Zhang, S., Zhang, X., Li, Y., & Guo, X. (2019). Bottom and Intermediate Nepheloid Layer Induced by Shoaling Internal Solitary Waves: Impacts of the Angle of the Wave Group Velocity Vector and Slope Gradients. *Journal of Geophysical Research: Oceans*, *124*(8), 5686–5699. https://doi.org/10.1029/2018JC014721

Wickham, H., Averick, M., Bryan, J., Chang, W., McGowan, L. D., François, R., et al. (2019). Welcome to the Tidyverse. *Journal of Open Source Software*, *4*(43), 1686. https://doi.org/10.21105/joss.01686

Woodward, E. M. S., & Rees, A. P. (2001). Nutrient distributions in an anticyclonic eddy in the northeast Atlantic Ocean, with reference to nanomolar ammonium concentrations. *Deep Sea Research Part II: Topical Studies in Oceanography*, *48*(4), 775–793. https://doi.org/10.1016/S0967-0645(00)00097-7